© Universiti Tun Hussein Onn Malaysia Publisher's Office

IJIE

Journal homepage: http://penerbit.uthm.edu.my/ojs/index.php/ijie
ISSN : 2229-838X e-ISSN : 2600-7916

The International Journal of Integrated Engineering

Spectrum Absorbency of Metamaterial Perfect Absorber

Siti Adlina Md Ali[1*], Maisarah Abu[1], Siti Normi Zabri[1]

[1]Centre for Telecommunication Research and Innovation, Fakulti Kejuruteraan Elektronik & Kejuruteraan Komputer, Universiti Teknikal Malaysia Melaka, MALAYSIA

*Corresponding Author

DOI: https://doi.org/10.30880/ijie.2022.14.01.019
Received 11 August 2021; Accepted 21 December 2021; Available online 07 March 2022

Abstract: A triple-band metamaterial perfect absorber was introduced. The single and simple structure based on gold-bar shaped was designed on the 0.018λ Taconic TLY-5. The gold-bar shaped was designed horizontal initially was then being rotated anti-clockwise from 0º to 90º to analyze and understand the change of absorption graph. Dual-band perfect metamaterial absorber was achieved at 45º. The fundamental and third harmonic magnetic resonances caused the low and high frequency peaks, respectively. Then, the gold-bar shaped was slotted at both end to create triple-band metamaterial perfect absorber. The slotted gold-bar shaped was evaluated in three absorption peaks: 99.94%, 99.88% and 99.66% at 3.98 GHz, 4.81 GHz and 5.33 GHz, respectively. This, however, moved to the 3.96 GHz, 4.80 GHz and 5.33 GHz with absorbency 99.79%, 99.95% and 99.90% for the measured structure. Both simulated and measure results were achieved absorbency over 99%, which was almost perfect absorption (≈100%). These properties are expected to be used in real-world applications such as satellite and radar communications transmission, particularly in lowering radar cross-section for stealth applications.

Keywords: Triple-band, absorption spectrum, perfect absorber, slotted gold-bar shaped

1. Introduction

Various types of perfect metamaterial absorber (MA) have been proposed since the first report on perfect MA [1]. Thus were single-band [2-3], multi-band [4-6], wideband [7-9], polarization-insensitive [10-11], and flexible [12] [20]. The MA was created in general by minimising reflection and eliminating transmission. The great majority of them consist of two metallic layers separated by a dielectric substrate. Impedance matching was used to reduce reflection by placing the patch on top of the dielectric. Meanwhile, to prevent transmission within the structure, the ground plane was printed as a continuous metallic layer on the bottom of the dielectric.

The absorber was one of these metamaterial applications for which no natural characterization exists. A planar MA was typically composed of a patterned metallic layer separated by a dielectric layer and a metallic ground plane. The metallic ground plane obstructed the transmission. Simultaneously, by adjusting the permittivity and permeability, the reflection is minimised depending on the impedance matching between surface impedance $Z(\omega)$ and free space impedance, $\eta_o = 377\ \Omega$, by adjusting the permittivity and permeability.

The metamaterial absorber is theoretically perfectly matched, which is the fundamental principle for maximizing absorbency. Since the free space impedance contributes almost nothing to reflection, there is no reflection and maximum absorbance, as occurred in equation 1

$$A = 1 - \left|S_{11}\right|^2 - \left|S_{21}\right|^2 \quad (1)$$

where S_{11} is reflected power and S_{21} is transmitted power. Due to the general full metal layers at the bottom of the structure, the transmitted power of the absorber is close to zero. Ideally, no transmission power should be transmitted at the back, since $S_{21} \approx 0$. Therefore, the absorbance, A is simplified as in equation 2

*Corresponding author: p021810003@student.utem.edu.my

$$A = 1 - |S_{11}|^2 \quad (2)$$

where A is absorbency, S_{11} is reflection coefficient and S_{21} is transmission coefficient.

Surface current at the front and back layers, magnetic energy, electric energy, and power loss at the resonant frequency were all proposed in 2015 [13]. On the front layer, the surface current was flowing bottom-up. Contributed to anti-parallel surface currents, indicating magnetic resonance; induced on top and bottom layers. The magnetic resonance was caused by electric energy distributions and power loss. The incident EM wave loss was dissipated within the dielectric space between neighbouring unit cells. The practical capacitors that were formed were primarily responsible for the induced electric field. In other words, using magnetic resonance, the dielectric loss dominates the energy dissipation of this MPA.

Meanwhile, the T-shaped, split-I (SI)-shaped and split-Jerusalem cross (SJC)-shape [2]. Single-band MA was developed with a T-shaped structure was then continued with SI-shaped for dual-band and SJC-shaped for multi-band MA. However, the performances of the three types MA proposed were not maintained the absorbency to be as a perfect MA at each resonance frequency. A simple patch (I-shaped) was built for a single-band, initially being scaled to a complex structure of SJC-shaped to develop multi-band MA.

In this paper, we investigated a triple-band metamaterial perfect absorber was introduced. The single and simple structure based on gold-bar shaped was designed on the 0.018λ Taconic TLY-5. The gold-bar shaped was designed horizontal initially was then being rotated anti-clockwise from 0° to 90° to analyze and understand the variation of absorption spectrum. Dual-band perfect metamaterial absorber was achieved at 45°. Then, the gold-bar shaped was slotted at both end to develop triple-band metamaterial perfect absorber.

2. Methodology

Multi-band MA was created using a simple gold-bar shape structure. Between the printed metal and the entire ground plane was a dielectric substrate. Taconic TLY-5 (thickness 1.52 mm, dielectric constant 2.2, and tangent loss 0.0009) and copper (0.035 mm thickness) were chosen as dielectric and metal materials, respectively.

Initially, a single and simple structure based on a gold-bar was designed. Then, the gold-bar being rotated anti-clockwise from 0° to 90° to study and interpret the change of the absorption graph. Then the design of the curve, which was slotted at both ends of the gold-bar, as being rotated at 45°. The optimized unit cell had dimensions of m_x = 45 mm and n_y = 48 mm in the x-y plane, and the thickness of the dielectric substrate was 0.018λ in the propagation direction-z. Meanwhile, x = 18 mm and y = 39 mm were the gold-bar's width and length, respectively. The curve that was slotted at both ends of gold-bar has width, w of 0.5 mm. Fig. 1 proposed unit cell of multi-band slotted gold-bar MA where Fig. 1 (a) shows the gold-bar, Fig. 1 (b) shows the rotated gold-bar at 45° and Fig. 1 (c) shows the slotted gold-bar.

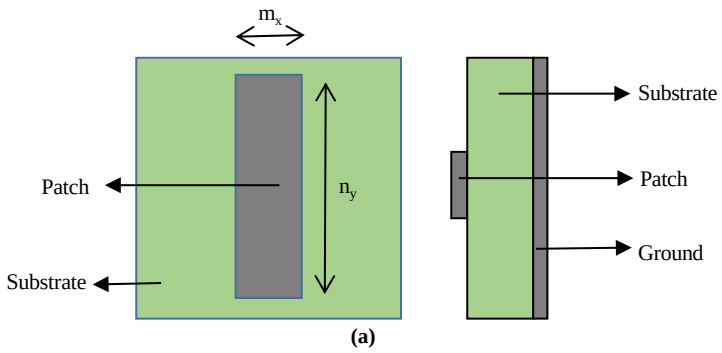

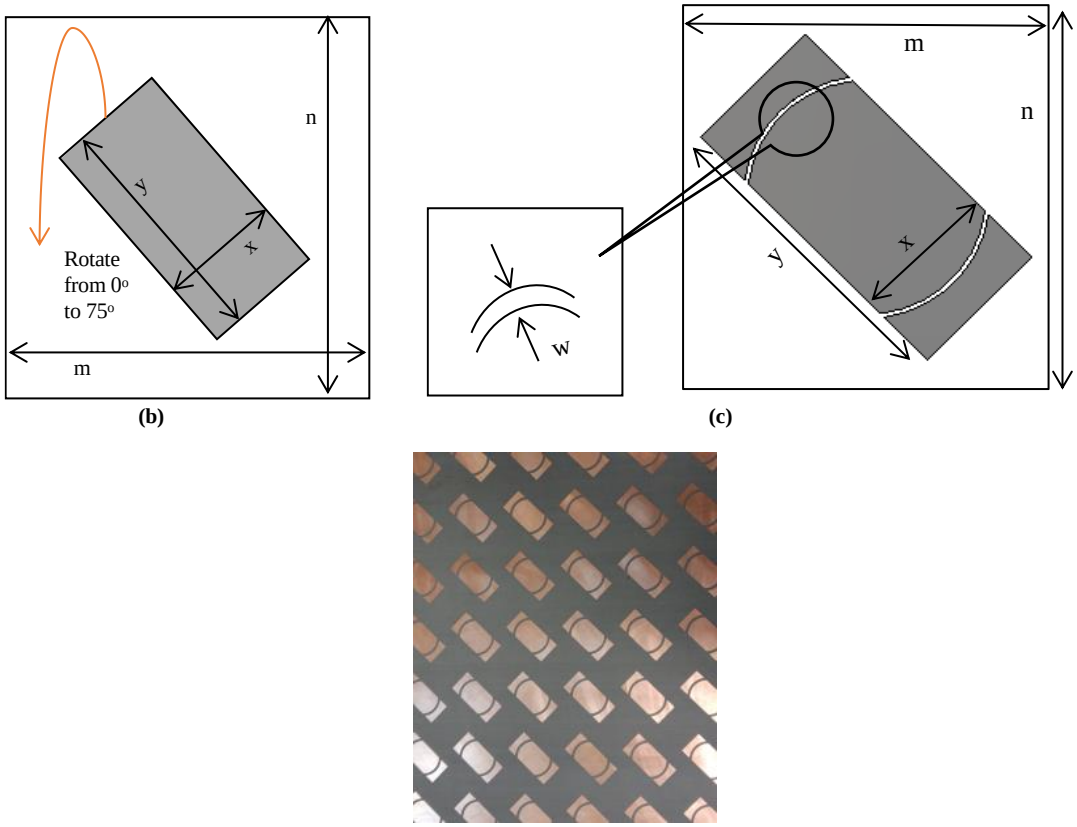

Fig. 1 - Triple-band MA (a) the gold-bar; (b) the rotated gold-bar at 45°; (c) the slotted gold-bar; (d) fabricated structure

3. Results and Discussion

Fig. 2 shows the single band MA gold-bar patch, and Fig. 2 (a) shows the reflection and absorbency of the single band MA gold-bar patch. The structure was operated at 2.50 GHz with 10.74% of absorbency capability. Thus, a - 0.49 dB of reflection contributed, which was not good enough to work as an MA in real life applications. The real and imaginary parts of normalized impedance were achieved approximately at one and zero, respectively, as plotted in Fig. 2 (b).

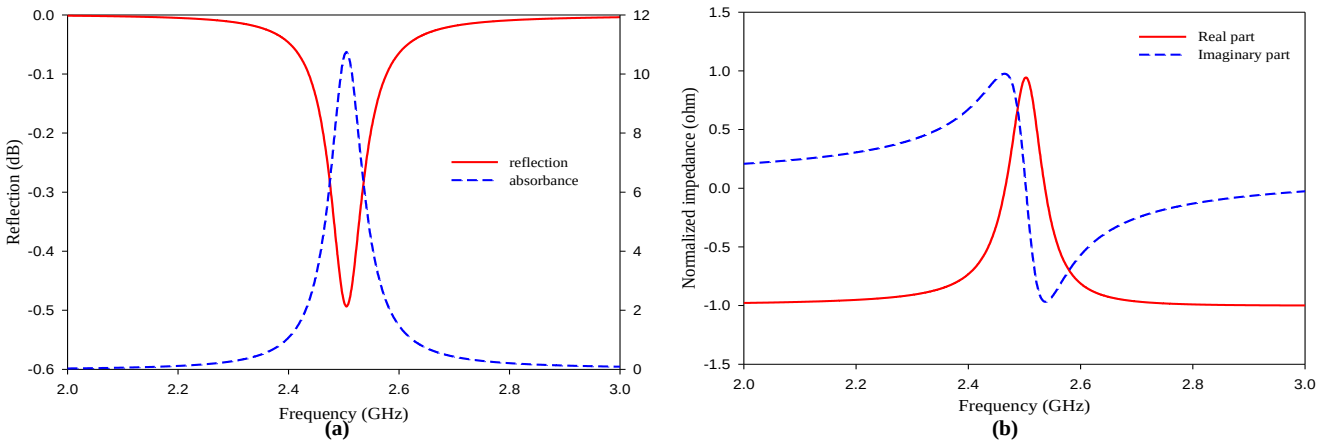

Fig. 2 - Single-band MA gold-bar patch (a) the reflection and absorbency; (b) the normalized impedance

The low and high frequency peaks were caused, respectively, by the fundamental and third harmonic magnetic resonances. Equations 3 until equation 5 were explained the resonance frequency of the triple-band MA.

$$k_{mn} = \frac{\omega_{mn}\sqrt{\varepsilon}}{c} = \frac{\pi}{l}\sqrt{m^2 + n^2} \quad (3)$$

$$\omega_{mn} = 2\pi f_{mn} \quad (4)$$

$$f_{mn} = \frac{c\sqrt{m^2 + n^2}}{2l\sqrt{\varepsilon}} \quad (5)$$

where, k_{mn} was resonance modes, n and m are integers (0, 1, 2...), and l was the length of bar patch.

The first resonance was occurred at 2.59 GHz indicate that the absorption was induced by the fundamental magnetic resonance (m = 1, n = 0). On the other hand, the second resonance was occurred at 5.18 GHz, which correspond to the second harmonic magnetic resonance (m = 2, n = 0). Two of the calculated resonance frequencies were very close to the simulated ones. The single-band MA gold-bar patch was designed horizontally, then rotated anti-clockwise from 0º to 90º to study the change of the absorption graph. Fig. 3 shows the absorption curves according to the anti-clockwise rotation of the MA gold-bar patch. Single-band occurred at both 0º and 90º with almost 10% of absorption. At the same time, a dual-band absorber was determined as the gold-bar was rotated from 15º up to 75º. The absorption for dual resonating frequencies was around 30% at both 15º and 75º of the rotation. Meanwhile, 80% of absorption was achieved at the rotation of 30º and 60º. Dual band MA gold-bar patch was achieved as the gold-bar was rotated at 45º at both bands: 2.50 GHz and 4.97GHz, with the absorption of 99.92% and 99.95%, respectively.

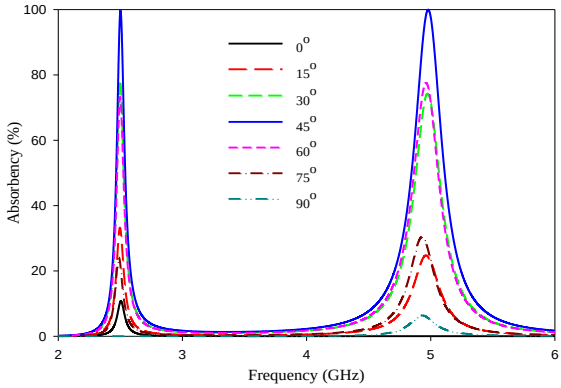

Fig. 3 - The absorption spectra of MA gold-bar patch

To investigate the in-depth variation of the spectra at 45º rotation, detailed absorption spectra at rotation angles ranging from 40º to 45º were simulated, as shown in Fig. 4. The absorbance capability of both bands increased as the rotation angle of the rectangular bar was changed from 40º to 45º. The absorptions were found to be relatively high at a rotation of 45º; the absorption of the first band was 99.50% at 2.50 GHz, and the absorption of the second resonance band was 99.95% at 4.97 GHz.

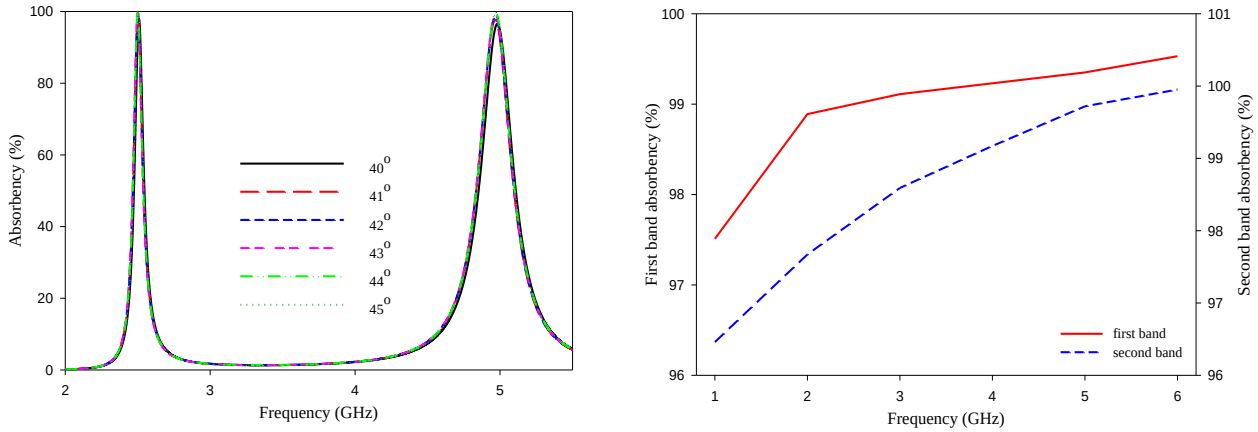

(a) **(b)**

Fig. 4 - Simulated absorption spectra of MA bar patch: (a) for rotation angles from 40º to 45º; (b) at 45º for first band and second band

Because dielectric loss was the dominant loss process for the absorption mechanism, the thickness of the dielectric substrate was varied to improve absorption of all resonance peaks. The dielectric substrate thickness was adjusted based on market availability; 0.09 mm, 0.25 mm, 0.76 mm, and 1.52 mm at a fixed rotation angle of the rectangular bar of 45°.

Fig. 5 (a) presents the absorption graph by the thickness of the dielectric substrate. For the first resonance peak, the frequency was moved from 2.50 GHz for 1.52 mm to 2.56 GHz for 0.09 mm thickness. At the same time, it was slightly moved to the upper side for the high-frequency absorption, which was from 4.98 GHz to 5.38 GHz with 99.95% and 94.35% absorbency, respectively. The absorbency was enhanced as the thickness of the dielectric was increased for both resonance peaks. It is also noted that the thicker dielectric contributed to the enhancement of bandwidth for each resonance peak.

Fig. 5 (b) and Fig. 5 (c) show the resonance frequencies for each band and Q-factor as a function of dielectric thickness. The first and second peaks were both shifted to higher frequencies. As a result, the resonance frequency was inversely proportional to the dielectric substrate thickness. The calculated Q-factor was reduced with dielectric thickness for the first and second peaks, resulting in a wider bandwidth. According to these findings, despite the fact that the dielectric substrate was slightly thick, the dielectric thickness was responsible for the wide dual peaks.

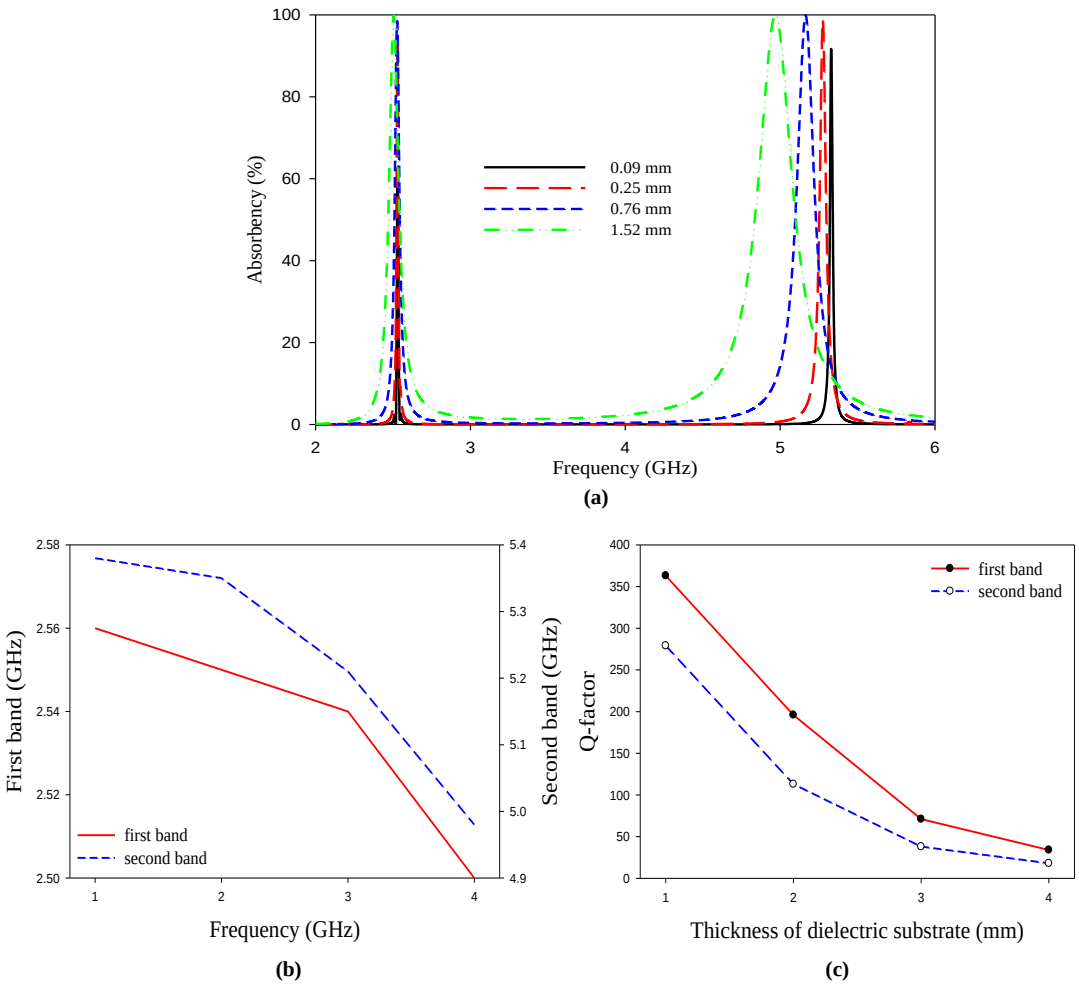

Fig. 5 - Rectangular gold-bar rotated at 45°: (a) simulated absorption graph according to the dielectric thickness; (b) resonance frequencies for each peak; (c) Q-factor according to the dielectric thickness

The gold-bar, which was rotated at 45°, was then slotted with a 0.45 mm curve at both ends of the structure, named multi-band MA gold-bar patch. The simulated and measured results for the reflection and absorbency of the proposed MA gold-bar patch were shown in Fig. 6 (a) and Fig. 6 (b), respectively. As aforesaid, the simulation result shows three absorption peaks: 99.94%, 99.88%, and 99.66% at 3.98 GHz, 4.81 GHz, and 5.33 GHz, respectively. This, however, moved to 3.96 GHz, 4.80 GHz, and 5.33 GHz with absorbency 99.79%, 99.95%, and 99.90% for the measured structure. Both simulated and measure results were achieved absorbency over 99%, which was almost perfect absorption (≈100%). The difference between simulated and measured results was caused by substrate non-uniformity and free space measurement tolerances. The surface current distribution on both the top and bottom metal layers at each operating frequency was observed to better understand the multi-band MA gold-bar patch.

Fig. 7 shows the simulated input impedance of the proposed multi-band MA gold-bar patch. The real part of input impedance was 0.99, 0.96 and 0.94 while the imaginary part of input impedance was 0.04, -0.05 and 0.02 at 3.98 GHz, 4.81 GHz, and 5.33 GHz respectively. It was discovered that at three distinct absorption peaks, the imaginary and real parts' impedance matching are approximately unity and zero, respectively. It was discovered that the imaginary and real parts' impedance matching are approximately unity and zero at three distinct absorption peaks. Furthermore, the input impedance reveals that the proposed structure's surface input impedance and free space impedance are well matched to 377 Ω and 0 Ω.

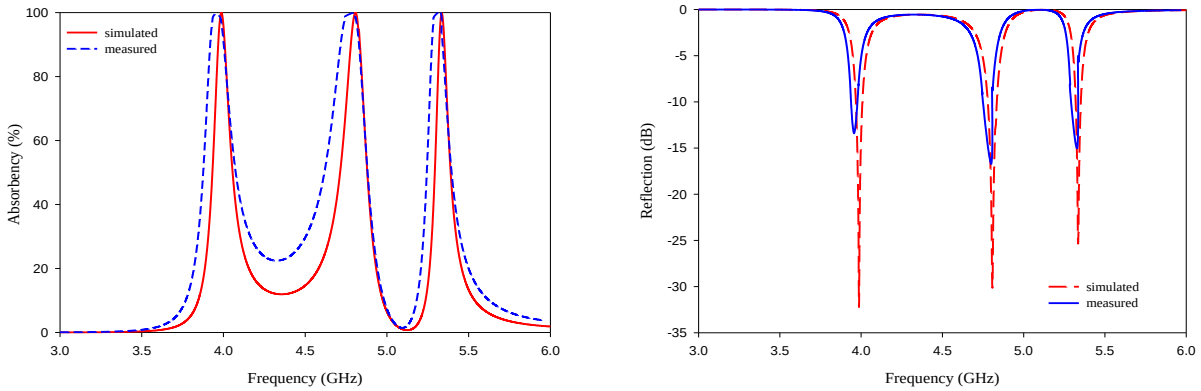

Fig. 6 - Simulation and measurement of the proposed multi-band MA gold-bar patch: (a) reflection and (b) absorbency

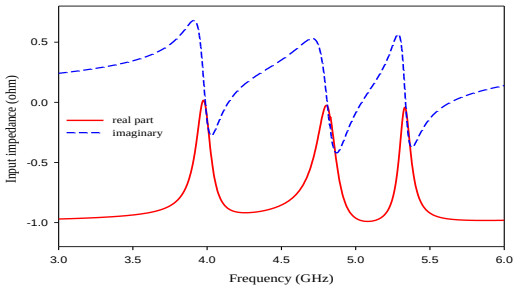

Fig. 7 - Simulated input impedance of multi-band MA gold-bar patch

The induced surface currents at all resonance frequencies were simulated to better understand the absorption mechanism. Fig. 8 depicts the distribution of anti-parallel surface currents on the front and back metallic layers for each peak. The absorption at the first peak, 3.98 GHz, was caused by anti-parallel surface currents between the front and back metal layers on both sides of the major rectangular part. Furthermore, anti-parallel surface currents at both ends of the minor rectangular parts caused absorption at the second peak, 4.81 GHz. The third absorption peak, on the other hand, depicts anti-parallel surface currents between the rectangular bar's major and minor parts' front and back metallic layers. Anti-parallel surface currents in various-size resonators induced multi-band perfect absorbers in the previous general.

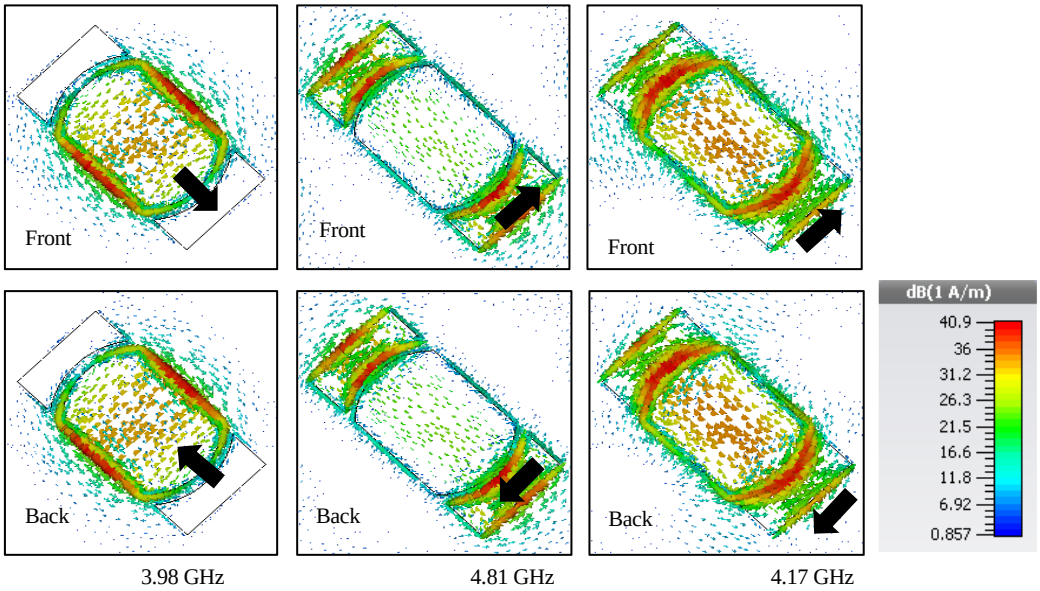

Fig. 8 - Current surface, power loss distribution of multi-band MA gold-bar patch

In terms of unit cell size, substrate thickness, and absorbency, the proposed multi-band MA gold-bar patch, which was designed on the basis of a slotted bar patch, was compared to some representative previous absorbers. The comparisons were based on the shortest possible working wavelength, λ_{fL}. As shown in Table 1, the proposed multi-band MA gold-bar patch was compact compare to [15] and the substrate was thinner than [17]. Most of the previous studies used a common FR-4 board which was a lossy dielectric material, contributed to the loss of the absorber itself. However, the proposed absorber was considered bigger in unit cell size and thicker substrate as compared to the Polyimide [18-19] and Teflon [20] dielectrics. The novelty of this proposed project was having an almost perfect absorbency in each of the resonance frequency, contributing to an efficient applications.

Table 1 - Review on multi-band MA gold-bar patch

Reference	Unit cell size	Substrate thickness	Absorbency, A (%)
[14]	0.011λ	0.111λ	- 95, 95.9, 95.4
[15]	0.053λ	0.001λ	- 99.37, 97.18
[16]	0.011λ	0.009λ	- 6 bands with A > 97
[17]	0.017λ	0.020λ	- 4 bands with A > 98
[18]	0.001λ	0.001λ	- Wide-band with A > 90
[19]	0.0002λ	0.001λ	- Wide-band with A > 97
[20]	0.009λ	0.009λ	- 5 bands with with A > 87
This project	0.025 λ	0.018λ	- 99.94, 99.88, 99.66

4. Conclusion

A triple-band metamaterial perfect absorber was successfully designed. The single and simple structure based on gold-bar shaped was designed on the 0.018λ Taconic TLY-5. The gold-bar shaped was designed horizontal initially was then being rotated anti-clockwise from 0° to 90° to analyse and understand the variation of absorption spectrum. Dual band perfect metamaterial absorber was achieved at 45°. Then, the gold-bar shaped was slotted at both end to develop triple-band metamaterial perfect absorber. The slotted gold-bar shaped was evaluated three absorption peaks: 99.94%, 99.88% and 99.66% at 3.98 GHz, 4.81 GHz and 5.33 GHz, respectively. This however, shifted to the 3.96 GHz, 4.80 GHz and 5.33 GHz with absorbency 99.79%, 99.95% and 99.90% for the measured structure. Both simulated and measure results were achieved absorbency over 99% which was almost perfect absorption (≈100%). These properties are expected to be used in practical applications such as satellite and radar communications transmission, specifically in reducing radar cross section for stealth applications.

Acknowledgement

The support of Universiti Teknikal Malaysia Melaka (UTeM) is greatly acknowledged. The research has been funded by UTeM Zamalah Scheme.

References

[1] Landey, N. I., Sajuyigbe, Mock, J. J., Smith, D. R., and Padilla, W. J. (2008). Perfect Metamaterial Absorber. Physical Review Letter, 100(20), 207402.
[2] Jain, P., Singh, A. K., PAndey, J. K., Garg, S., Bansal, S., Agarwal, M., Kumar, S., Sardana, N., Gupta, N., and Singh, A. K. (2019). Ultra-Thin Metamaterial Perfect Absorber for Single-Dual-Multiband Microwave Applications, IET Microwaves, Antenna and Propagation, 14(5), 390-396.
[3] Feifei, L., Chao, M., Fanguang, M., Digang, F., Ping, C., and Rui-Xin, W. (2018). A Thin Broadband Microwave Absorber with Hexagonal Resistive Frequency Selective Surface. IEEE Antennas and Wireless Propagation Letters. 1-5.
[4] Ji, S., Jiang, C., Zhao, J., Zhang, X., and He, Q. (2018). Design of a Polarization-Insensitive Triple-Band Metamaterial Absorber. Optics Communications.
[5] Kaur, M., and Singh H. S. (2019). Design and Analysis of a Compact Ultrathin Polarization and Incident Angle Independent Triple Band Metamaterial Absorber. Microwave Optical Technology Letters, 1-9.
[6] Wu, J., Zahang, F., Li, Q., Chen, J., Feng, Q., and Wu, L. (2020). Infrared Five Band Polarization Insensitive Absorber with High Absorptivity Based on Single Complex Resonator. Optics Communications, 456, 1-5.
[7] Yu-Long, Z., Xiang-Yu, C., Jun, G., Yeu-Jun, Z., Huan, Y., and Si-Jia, L. (2019). Broadband Aperture-Coupling Patch Antenna with Improved Radiation and Scattering Performance based on Metamaterial Absorber. IET Microwaves, Antenna and Propagation. 13(7), 875-880.
[8] Singh, H. S. (2019). Super Compact Ultrathin Quad-Band with Wide Angle Stability Polarization Independent Metamaterial Absorber. Microwave Optical Technology Letters, 1-8.
[9] Thi, K. N., Thi, M. N., Hong, Q. N., Thanh, N. C., Dac, T. L., Xuan, K. B., Son, T. B., Chi, L. T., Dinh, L.V., and Thi, Q. H. N. (2021). Simple Design of Efficient Broadband Multifunctional Polarization Converter for X-Band Applications. Scientific Reports. 1-12.
[10] Mustapha, M. G., Rahim, M. K. A., Murad, N. A., Ayop, O., Tuntrakool, S., Baba, M. A., Iliyasu, A. Y. and Jalil, M. E. (2020). Polarization Insensitive Switchable Metamaterial Absorber/Reflcetor for X Band Applications. Bulletin of Electrical Engineering and Informatics. 9(6), 2443-2448.
[11] Mingbao, Y., Jiafu, W., Weiyu, W., Cuilian, X., Hongya, C., Wenjie, W., Lin, Z., and Shaobo, Q. (2021). An FSS-Backed Reflective Polarization Conversion Meta-Surface for Radar Stealth. Photonics and Nanostructures Fundamentals and Applications. 43 (2021), 1-7.
[12] Isa, S. N., Ayop, O, Supa'at, A. S. M., Rahim, M. K. A., Murad, N. A., Zubir, F., and Majid, H. A. (2020). Effects of Bending on a Flexible Metamaterial Absorber. Bulletin of Electrical Engineering and Informatics. 9(6), 2436-2442.
[13] Bui, X. K., Bui, S. T., Nguyen, V. D., Young, J. Y., Young, J. K., Ki, W. K., Vu, D. L., Jun, G. Y., and Young, P. L. (2015). Size-efficient Metamaterial Absorber at Low Frequencies: Design, Fabrication, and Characterization. Journal of Applied Physics, 117.
[14] Cao, H., Shan, M., Chen, T., Lei, J., Yang, L., & Tan X. (2019). Triple-Band Polarization-Independent Ultrathin Metamaterial Absorber. Progress in Electromagnteics Reseacrh M, 77, 93-102.
[15] Singh, H., Mittal, N., and Arora, O. (2020). Designing and Analysis of Frequency Reconfigurable Double negative Flower Leaf Metamaterial Absorber. Materials Today: Proceedings.
[16] Al-Badri, K. S. L. (2020). Electromagnetic Broad Band Absorber Based on Metamaterial and Lumped Resistance. Journal of King Arab Saudi University-Science, 32, 501-506.
[17] Lee, J., Yoo, M., and Lim, S. (2015). A study of Ultrathin Single Layer Frequency Selective Surface Microwave Absorbers with Three Different Bandwidth Using Double Resonance. IEEE Transactions on Antenna and Propagation, 63(1), 221-230.
[18] Bui, X. K., Bui, S. T., Young, J. K., Ki, W. K., Joo, Y. R., Vu, D. L., Liang, Y. C., and Young, P. L. (2019). Broadband and Ultrathin Metamaterial Absorber Fabricated on a Flexible Substrate in the Long-Term Evolution Band. Journal of Electronic Material.
[19] Kim, Y. J., Hwang, J. S., Khuyen, B. X., Tung, B. S., Kim, K. W., Rhee, J. Y., Chen, L. Y., and Lee, Y. P. (2018). Flexible Ultrathin Metamaterial Absorber for Wide Frequency Band, based on Conductive Fibers. Science and Technology of Advance Materials.
[20] Yoo, Y. J., Zheng, H. Y., Kim, Y. J., Rhee, J. Y., Kang, J. H., Kim, K. W., Cheong, H., Kim, Y. H., and Lee, Y. P. (2019). Flexible and Elastic Metamaterial Absorber for Low Frequency, Based on Small-Size Unit Cell. Applied Science. 105.